

Georgia State University

ScholarWorks @ Georgia State University

Chemistry Honors Theses

Department of Chemistry

Summer 7-18-2019

Characterization of the Proline-78-Glycine Mutant of PA1024 from *Pseudomonas aeruginosa*

Benjamin Dratch

Follow this and additional works at: https://scholarworks.gsu.edu/chemistry_hontheses

Recommended Citation

Dratch, Benjamin, "Characterization of the Proline-78-Glycine Mutant of PA1024 from *Pseudomonas aeruginosa*." Thesis, Georgia State University, 2019.

doi: <https://doi.org/10.57709/15011646>

This Thesis is brought to you for free and open access by the Department of Chemistry at ScholarWorks @ Georgia State University. It has been accepted for inclusion in Chemistry Honors Theses by an authorized administrator of ScholarWorks @ Georgia State University. For more information, please contact scholarworks@gsu.edu.

Characterization of the Proline-78-Glycine Mutant of PA1024

from *Pseudomonas aeruginosa*

by

Benjamin Deen Dratch

Under the Direction of Dr. Giovanni Gadda

Abstract

NAD(P)H:quinone oxidoreductases (NQOs) are flavin-dependent enzymes that catalyze the two-electron reduction of quinones and the oxidation of NAD(P)H. NQOs play a role in cellular detoxification by preventing the formation of radical quinones thus avoiding the generation of reactive oxygen species. The NQO from *Pseudomonas aeruginosa* PAO1 (PA1024) is proposed to serve a dual function in the cell by detoxifying quinones and balancing the [NAD⁺]/[NADH] ratio. Crystal structures of wild-type PA1024 were previously solved in free form and in complex with NAD⁺ (PDB: 2GJN & 6E2A). Comparison of the ligand-free and ligand-bound structures of the enzyme reveals a loop (residues 75-86) in two conformations, suggesting the mobile loop may play a role in NADH binding and selectivity. P78 is located on the mobile

loop and is hypothesized to provide internal rigidity to the mobile loop to help carry out its functions. In the present study, site-directed mutagenesis was utilized to replace P78 with glycine and increase mobile loop flexibility. The mutant (NQO-P78G) was expressed and purified as previously described for wild-type PA1024. Apparent steady-state kinetics of NQO-P78G, at varying concentrations of benzoquinone and a fixed [NADH] of 0.1 mM, showed a 20-fold reduction in the k_{cat} value with respect to the wild-type enzyme, i.e., 1.3 s^{-1} vs. 27 s^{-1} . When the concentration of NADH was varied with a fixed [benzoquinone] at 21 μM , NQO-P78G could not be saturated and only a $k_{\text{cat}}/K_{\text{NADH}}$ value of $11,000 \pm 700 \text{ M}^{-1} \text{ s}^{-1}$ could be determined. On the basis of kinetic results presented here, we propose that P78 does not play a role in substrate specificity but rather it is important in assisting with catalysis in PA1024.

INDEX WORDS: PA1014, Substrate specificity, Mobile loop, NADH, Quinone Reductase

Characterization of the Proline-78-Glycine Mutant of PA1024

from *Pseudomonas aeruginosa*

by

Benjamin Deen Dratch

An Honors Thesis Submitted in Partial Fulfillment of the Requirements for the Degree of

Bachelor of Chemistry

in the College of Arts and Sciences and Honors College

Georgia State University

2019

Copyright by
Benjamin Deen Dratch

Characterization of the Proline-78-Glycine Mutant of PA1024
from *Pseudomonas aeruginosa*

An Honors Thesis

Presented in Partial Fulfillment of Requirements for the Degree of Bachelor of Chemistry in the
College of Arts and Sciences and Honors College

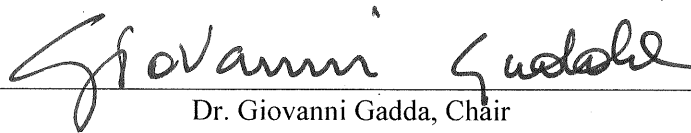
Georgia State University

2019

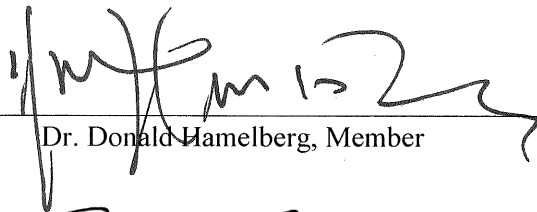
by

Benjamin Deen Dratch

Committee:



Dr. Giovanni Gadda, Chair




Dr. Donald Hamelberg, Member



Dr. Samer Gozem, Member

7/18/19

Date



Dr. Donald Hamelberg
Department Chair

DEDICATION

This thesis is dedicated to all of my friends and family. Thank you for helping me get this far, I sincerely appreciate it. This is just the first of what is yet to come.

ACKNOWLEDGEMENTS

I would like to thank my advisor, Dr. Giovanni Gadda, for introducing me to the world of biochemical research and for pushing me to create this thesis. I have certainly grown more than I expected to in this past year. I am thankful for my committee members, Dr. Donald Hamelberg and Dr. Samer Gozem, for providing insightful criticisms and helping me find direction in my future research. I would also like to thank all of the lab members who have taught me and helped me grow during my stay in this lab. Chris, Archana, Renata, Dan, Daniel, Joanna, and Maria, you have all helped me in one way or another and I sincerely thank you. Chris, thank you for mentoring me when I first joined the lab and was still very new to everything the research world had to offer. You have all been a great help to me, thank you.

Introduction

Among the wide variety of protein structures discovered in nature, as much as 10% of enzymes are thought to contain a triosephosphate isomerase (TIM) barrel fold establishing it as the most common tertiary enzyme fold¹⁻³. The TIM-barrel fold is a type of β -barrel composed of eight parallel β -strands at the center of the fold and eight α -helices with $\beta\alpha$ and $\alpha\beta$ loops connecting the secondary structures¹. Sequence analysis of the TIM-barrel fold discovered the fold to be associated with 16 sequence families revealing that the fold could function as an oxidoreductase, transferase, lyase, hydrolase, or isomerase^{1, 4-6}. Active site residues that allow the fold to serve a variety of functions are found at the C-terminal ends of the β -stands and the adjacent loops ($\beta\alpha$ loops) while the remainder of the fold serves to provide stability to the enzyme⁶. $\beta\alpha$ loops are thought to be especially important for the activity of a TIM-barrel fold containing enzyme as they have been reported to have variable lengths implying the active site geometry is largely affected by these loops¹. Since the fold can be subdivided into ‘activity’ and ‘stability’ subunits it is possible to mutate or replace the $\beta\alpha$ loops without a loss in stability⁶⁻⁸. Experiments focused on mutating residues to learn more about the structure function relationship in proteins can easily be utilized for TIM-barrel fold containing enzymes as mutations on active site residues will not denature the protein^{6, 9}. Previous studies have utilized this methodology and have discovered it is possible to drastically change the function of an enzyme from just a single point mutation at a TIM-barrel fold’s β -strand C-terminus¹⁰.

Site-directed mutagenesis in combination with enzyme kinetics can elucidate the importance of residues in catalysis⁹. This methodology is used by mutating a residue on an enzyme and measuring kinetic parameters, as described by Michaelis-Menten kinetics¹¹, to describe the enzymatic reaction of the mutant enzyme in comparison to the wild-type enzyme¹². This

experimental process has been previously described in PaDADH¹³ and choline oxidase¹⁴. The Michaelis-Menten model describes enzyme kinetics using the kinetic parameters k_{cat} , K_M , and k_{cat}/K_M . To measure Michaelis-Menten parameters three requirements must be met; initial velocities must be measured, the concentration of substrate must be much greater than the concentration of enzyme, and the rate of reaction must be proportional to the concentration of the enzyme-substrate (ES) complex¹¹. The kinetic parameter k_{cat} is determined by the kinetic rate constants starting from the ES complex to product release¹⁵. Thus, k_{cat} describes the rate at which the enzyme turns over. The Michaelis-Menten constant, K_M , describes the concentration of substrate at which the rate of reaction is half of the maximum rate of reaction. Lastly, the kinetic parameter k_{cat}/K_M is determined by the kinetic rate constants starting from free enzyme up to and including the first irreversible step. Thus, k_{cat}/K_M describes how much total enzyme is engaged in what will become a catalytic event and can be simply described as ‘catalytic efficiency’¹⁵. By using Michaelis-Menten kinetics in conjuncture with mutagenesis it becomes possible to understand how changes in an enzymes sequence can alter certain aspects of an enzyme’s catalytic activity.

Quinone reductases (QRs) are flavin-dependent enzymes that catalyze two strict hydride transfers: the first is from NAD(P)H to the flavin cofactor and the second from the flavin to a quinone¹⁶. The purpose of a QR’s two electron transfer onto quinones is to ensure the formation of a hydroquinone while avoiding a one electron transfer which would result in a semiquinone radical^{16, 17}. Semiquinone radicals react with molecular oxygen to form reactive oxygen species which lead to symptoms caused by oxidative stress such as tissue degeneration, apoptosis, premature aging, and neoplasia^{18, 19}. It is thought that QRs play an important role in cellular detoxification by avoiding the generation of these harmful quinone species. QRs accept a variety of ring containing compounds meaning a single QRs can react with multiple forms of quinones as

well as nitro-aromatic compounds²⁰, azodyes, and ferric iron^{16, 21}. Some QRs can utilize NADH and NADPH as their electron donor however other QRs, such as PA1024 from *P. aeruginosa* or AzoA from *Enterococcus faecalis*, were found to have a clear preference for NADH as the reducing substrate^{16, 22}. How this substrate specificity is created is unknown however the existence of a glycine rich structural sequence found in Rossmann and flavodoxin-like folds has previously been accredited to play a role in the reducing substrate specificity binding^{23, 24}.

PA1024 from *Pseudomonas aeruginosa* was recently kinetically characterized and classified as an NADH:quinone oxidoreductase as opposed to its old classification of a 2-nitropropane dioxygenase; a class of protein which is now known as nitronate monooxygenases (NMOs)^{25, 26}. PA1024 was reclassified when enzymatic turnover was measured to be 25 times larger with known substrates of NADH:quinone oxidoreductases compared to those of NMOs²⁵. Additional investigations supported the reclassification when the conserved motifs that define class I and class II NMOs were found to have no similarity to the six structural motifs found for PA1024^{26, 27}. To understand what reducing substrate PA1024 utilizes, the genomic context of the enzyme was analyzed which revealed the enzyme is located on an operon that codes for various enzymes that play a role in β -oxidation such as acyl-CoA dehydrogenases and acyl-CoA hydratase/isomerase (all hypothetical)²⁵. It was then speculated that PA1024 also plays a role in β -oxidation by oxidizing NAD(P)H to create a ratio of NAD(P)H/NAD(P)⁺ that would stimulate the cycle^{25, 28, 29}. Existing conserved motifs of PA1024 were compared to hypothetical proteins located in the GenBankTM which revealed ~500 hypothetical proteins sharing the same structural motifs as PA1024 allowing for the creation of a new class of NADH:quinone oxidoreductases²⁵.

PA1024 is a quinone reductase that has a clear preference for NADH over NADPH regarding the enzymes reducing substrate²⁵. A preference for NADH over NADPH was discovered when

enzymatic assays measuring turnover of PA1024 determined NADPH reacted at least ~3,500 times slower than NADH²⁵. Recently a crystal structure of PA1024 in complex with NAD⁺ was solved and compared to PA1024's ligand-free structure to observe how the enzyme's structure might change during ligand binding. The ligand-bound structure revealed a mobile $\beta\alpha$ loop (residues 75-86) from PA1024s TIM-barrel fold that moves 5.5 Å toward the active site with respect to the ligand-free structure (Figure 1)³⁰. Upon loop movement, glutamine-80 (Q80) is shifted to the entrance of the active site and a potential interaction with tyrosine-261 (Y261) is made³⁰. It is proposed that the significance of the mobile loop taking a closed conformation is to facilitate Q80-Y261 interactions which could act as a gate mechanism to seal the active site once the substrate is bound³⁰.

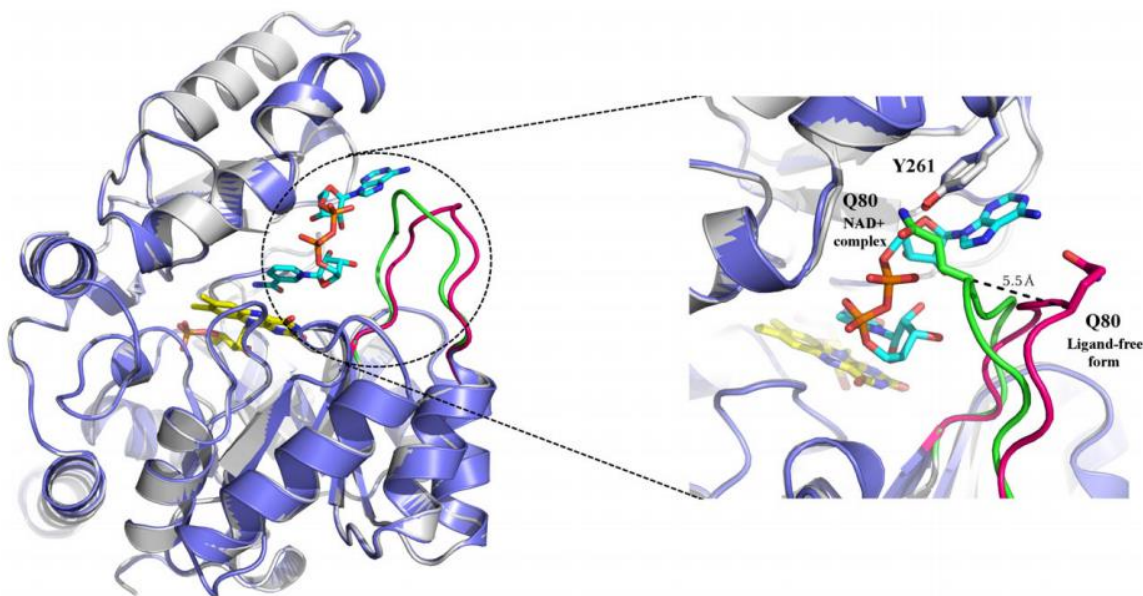


Figure 1. Superimposition of the ligand-free and NAD⁺ -complex structures of PA1024. The overall structure of the ligand-free form of PA1024 (PDB ID: 2GJL) is in blue and the PA1024-NAD⁺ complex (PDB ID: 6E2A) is in grey. The loop residues 75–86 are highlighted in pink (ligand-free form) and green (PA1024-NAD⁺ complex). The FMN carbons are in yellow sticks and the NAD⁺ carbons are in cyan. The dashed line represents the distance between the position of the C atom of Q80 in the ligand-free and NAD⁺ -complex structures. From “Steric hindrance controls pyridine nucleotide specificity of a flavin- dependent NADH:quinone oxidoreductase,” by Ball J. and Gadda G., 2018, *Protein Sci.*, Volume 28, p. 167-175. Copyright 2018 by The Protein Society. Reprinted with permission.

A subsequent theoretical model of PA1024 in complex with NADP⁺ was produced which tested various conformations of the phosphate group (Figure 2)³⁰. A comparison of PA1024 in complex with NAD⁺ and NADP⁺ suggests that the reducing substrate specificity results from steric hindrances on nearby residues rather than ionic interactions³⁰. The PA1024-NADP⁺ model shows that the 2' phosphate of NADP⁺ is blocked from the active site via steric hindrances with PA1024 residue's proline-78 (P78) and Q80³⁰. P78 and Q80 are located on the mobile loop suggesting that PA1024 cannot properly accept NADPH for it sterically hinders the closed conformation from forming. P78 is thought to not only sterically hinder NADPH but may also serve to provide rigidity to the mobile loop to help ensure Q80 interactions associate properly. A short section of the mobile loop (residues 66-78) is found to be highly conserved as part of the second structural motif of PA1024. On the second structural motif, P78 is found to be highly conserved among the ~500 hypothetical proteins that share the same conserved motifs at PA1024. The bioinformatic, structural, and kinetic characterizations of PA1024 all seem to hint that P78 plays an important role in creating a reducing substrate specificity for NADH:quinone oxidoreductases^{25, 30}.

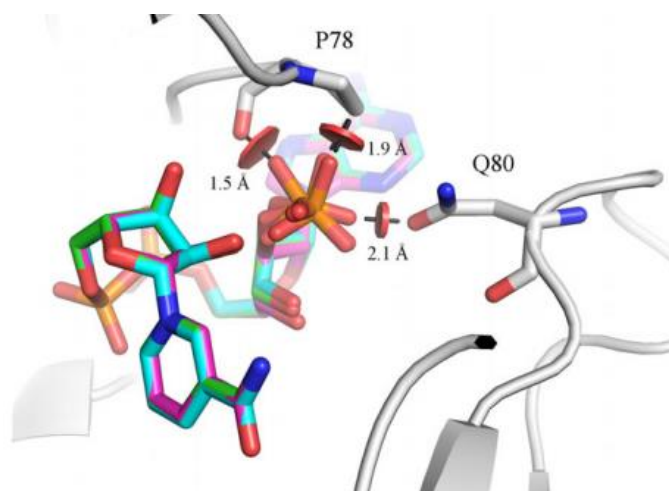


Figure 2. Model of hypothetical PA1024–NADP⁺ complex. Different conformations of the phosphate group in the NADP⁺ were modeled. The NADP⁺ carbons are in green, cyan and pink sticks, and the P78 and Q80 carbons and nearby loops of PA1024 are in grey. The red circles represent steric clashes with their respective distances between clashing atoms. From “Steric hindrance controls pyridine nucleotide specificity of a flavin- dependent NADH:quinone oxidoreductase,” by Ball J. and Gadda G., 2018, *Protein Sci.*, Volume 28, p. 167-175. Copyright 2018 by The Protein Society. Reprinted with permission.

In this study, the hypothesized function of P78 in the FMN dependent NADH:quinone oxidoreductase PA1024 was tested by structurally altering the enzyme to reduce steric hindrances at residue 78. P78 was replaced with a glycine via site-directed mutagenesis (NQO-P78G) which altered the steric hindrances and structural rigidity found at residue 78 in wild-type PA1024. Data on resulting NQO-P78G was collected using spectroscopic and steady-state kinetic techniques to investigate the importance of a P78G mutation on the NAD(P)H substrate specificity in wild-type PA1024. If we removed the highly conserved proline and subsequent steric hindrances at position 78 then it is expected PA1024 will lose its ability to select between NADH and NADPH.

Material and Methods

Materials

The enzymes *Pfu* DNA polymerase and *DpnI* were from Stratagene (La Jolla, CA) and New England Biolabs (Ipswich, MA) respectively. QIAprep Spin Miniprep kit and QIAquick PCR purification kit were from Qiagen (Valencia, CA). SYBR[®] Safe DNA gel stain was from Thermo Fisher Science (Canton, GA). CutSmart Buffer and Deoxynucleotide (dNTP) Solution Mix was from New England Biolabs (Ipswich, MA). Oligonucleotides, containing the point mutation P78G, were customized and ordered from Sigma Aldrich (The Woodlands, TX). Isopropyl-1-thio- β -D-galactopyranoside (IPTG) was ordered from Promega (Madison, WI). HiTrap[™] Chelating HP 5 mL affinity column and prepacked PD10 desalting columns were purchased from GE Healthcare (Piscataway, NJ). NADH and NADPH disodium salts were purchased from VWR (Radnor, PA). All other reagents used were of the highest purity commercially available.

Site-directed Mutagenesis, Protein Expression, and Purification

Escherichia coli strain DH5 α , harboring a pET20b(+)/*pa1024*²⁵ plasmid, was grown on Luria–Bertani (LB) agar plates containing 100 μ g/mL of ampicillin for 17 h at 37 °C. These starter colonies were used to inoculate 5 mL of LB broth containing 50 μ g/mL ampicillin. Resulting liquid cultures were grown under the same conditions as the LB agar plates. Cells were collected via centrifugation at 10,000 *g* and 4 °C for 10 min. The plasmid harboring wild-type *pa1024* was isolated by using a QIAquick Spin Miniprep Kit (Qiagen) following the manufacturer’s protocol. Isolated plasmids were used as a template for polymerase chain reaction (PCR) while custom designed oligonucleotide primers carried the desired point mutation for the *pa1024* gene (Table 1). PCR was run with an initial denaturation step at 98 °C for 2 min, 25 cycles of melting at 98 °C for 30 s, annealing at 68 °C for 45 s, elongation at 75 °C for 10 min, and a final elongation step at 75 °C for 10 min. The PCR reaction mix contained ~50 ng template DNA, 2.5 U *Pfu* DNA polymerase, 0.2 μ M per each primer, 5% DMSO, and the manufacturer’s suggested concentrations for the dNTP mix and *Pfu* buffer with a final volume of 50 μ L. Resulting amplicons were analyzed with agarose gel electrophoresis (1x SYBR[®] Safe DNA gel stain, 0.4% agar). The PCR products were purified using the QIAquick PCR Purification Kit (Qiagen) following the manufacturer’s protocol. Methylated DNA was digested for 2 h at 37 °C in 1x CutSmart Buffer and 2 μ L of *DpnI*. The *DpnI* digested product was used to transform chemically competent DH5 α cells using the heat shock method. Resulting colonies were grown on LB agar plates, purified for their plasmid using the QIAquick Spin Miniprep Kit, and sent for sequencing at MacroGen Inc (Rockville MD). NQO-P78G was expressed in *E. coli* strain Rosetta(DE3)pLysS and purified through methods previously described for the wild-type enzyme²⁵. Purified PA1024-P78G was stored at –20 °C in 20 mM KP_i (pH 7.4), 200 mM NaCl, and 10% glycerol.

Table 1. Oligonucleotides used as mutagenic primers in order to amplify pET20b(+)/pa1024-P78G

Primer	Nucleotide Sequence	T _m	GC%
P78G-For	5'-CACCTGACCTTGT <u>TAGGC</u> ACGCAGAAGCCGGTGCC-3'	86.2	61.1
P78G-Rev	5'-CACCGGCTTCTGCGT <u>GCCT</u> AACAAGGTCAGGTTGAC-3'	84.3	58.3

*Nucleotide bases that replace the wildtype proline codon with a mutagenic glycine codon are underlined.

Spectroscopic Studies

Prior to spectroscopic studies, the enzymes were passed through a PD-10 desalting column to separate out contaminants and denatured proteins. Circular dichroic spectra were acquired for wild-type PA1024 and NQO-P78G using a Jasco (Easton, MD) J-1500 Circular Dichroism Spectrophotometer. Studies were conducted in the far-UV region (180–250 nm) at 20 mM KP_i (pH 7.0) and 200 mM NaCl, at 25 °C, and concentrations of protein of 0.1 mg/mL. A 1 mm path length quartz cuvette was used to acquire a single scan at a rate of 20 nm/min. Spectra of water and buffer were measured and used as blanks to account for their contributions to signal response in the enzyme spectra. Resulting CD spectra were smoothed by the Means-Movement method and analyzed using Jasco Spectra Analysis program.

Enzyme Assays

Steady-state kinetic parameters were measured with an Agilent Technologies (Santa Clara, CA) model HP 8453 PC diode-array spectrophotometer equipped with a thermostated water bath in 20 mM KP_i (pH 7.0), 200 mM NaCl, and 10% (v/v) glycerol, at 25 °C, using the method of initial rates. Reaction rates were measured by following NADH consumption at 340 nm, using $\epsilon_{340} = 6,220 \text{ M}^{-1} \text{ cm}^{-1}$ ^{31, 32}. The traditional approach to obtain the steady-state kinetic mechanism by varying the concentration of both NAD(P)H and benzoquinone could not be carried out due to low

$K_{\text{benzoquinone}}$ values and high K_{NADH} values. An apparent steady-state experiment was run with benzoquinone at substrate concentrations ranging from 3 to 100 μM and NADH at a concentration of 100 μM . The reaction was initiated by the addition of NQO-P78G at a final concentration of 300 nM. Turnover of NQO-P78G with NAD(P)H was measured through a steady-state experiment where NAD(P)H was tested at concentrations ranging from 30 to 300 μM , at saturating 1,4-benzoquinone (21 μM), and 300 nM of enzyme.

Data Analysis

Kinetic data were fit using KaleidaGraph software (Synergy Software, Reading, PA). The apparent steady-state kinetic parameters at varying concentrations of benzoquinone was determined by fitting the initial rates of reactions to the Michaelis-Menten equation (Equation 1) or to Equation 2 in cases where substrate inhibition was seen. Initial rates were measured by taking the initial velocity of the reaction (v_0) over the concentration of enzyme (e). $K_{\text{benzoquinone}}$ and K_{NADH} represent the Michaelis-Menten constants for benzoquinone and NADH respectively while k_{cat} represents the turnover number of the enzyme at saturating concentrations of both substrates. The kinetic parameter K_i is used to account for the effect substrate inhibition has on initial rates. Steady-state kinetic parameters at varying concentrations of NAD(P)H were fit to a Michaelis-Menten equation that measured true kinetic parameters (Equation 3). This equation is further derived from the Michaelis-Menten equation for two substrates after determining that the $K_{\text{benzoquinone}}$ is much smaller than the concentration of benzoquinone used so that $K_{\text{benzoquinone}}/[\text{benzoquinone}] = \sim 1$. Thus, it is possible to assume that all terms involving $K_{\text{benzoquinone}}$ have a negligible effect on v_0/e .

$$\frac{v_o}{e} = \frac{^{app}k_{cat} [\text{benzoquinone}]}{^{app}K_{\text{benzoquinone}} + [\text{benzoquinone}]} \quad (1)$$

$$\frac{v_o}{e} = \frac{^{app}k_{cat} [\text{benzoquinone}]}{K_{\text{benzoquinone}} + [\text{benzoquinone}] + \frac{[\text{benzoquinone}]^2}{K_i}} \quad (2)$$

$$\frac{v_o}{e} = \frac{k_{cat} [NADH]}{K_{NADH} + [NADH]} \quad (3)$$

Results

Site-directed Mutagenesis, Protein Expression, and Purification

pa1024-P78G and NQO-P78G were successfully prepared for further experimentation through a PCR on *pa1024* and protein purification as previously described²⁵. DNA sequencing results confirmed the inserted *pa1024* gene contained a P78G point mutation as well as an absence of undesired mutations. Mutagenic primers, a pET20b(+)/*pa1024* DNA template and *Pfu* DNA polymerase were utilized as the key components for a successful PCR. Custom designed primers were designed to contain the P78G mutation which, upon extension, produced the desired pET20b(+)/*pa1024*-P78G mutant plasmid. Addition of 5% DMSO to the PCR reaction mix was necessary due the high GC content of the *pa1024* gene. DMSO facilitates the denaturation of GC rich DNA regions during PCR to prevent the formation of unwanted secondary structures in the primers. Template plasmids were removed from the PCR product reaction mix through a *DpnI* restriction digest. *DpnI* endonucleases digest methylated nucleotide sequences and among the plasmids in the PCR product mix, only wild-type plasmids had been exposed to methylases in vivo. The pET20b(+) plasmid harboring *pa1024*-P78G was taken up by competent *E. coli* DH5 α cells using the heat shock method. The transformed pET20b(+)/*pa1024*-P78G plasmid was purified and sequenced to discern if the mutant plasmid was properly prepared. Through the NCBI

Nucleotide Blast program, sequencing results were compared to the wild-type sequence of *pa1024*. The nucleotide sequence alignment revealed the nucleotides at positions 232-234 were mutated from CCG to GGC which corresponds to a successful P78G mutation. Purified pET20b(+)/*pa1024*-P78G was taken up by competent *E. coli* Rosetta(DE3)pLysS cells as a first step to purifying NQO-P78G. NQO-P78G was purified to a high yield using the protocol for wild-type PA1024 thus, troubleshooting protein expression and purification was not necessary. The storage buffer for NQO-P78G was 20 mM KP_i (pH 7.0) and 200 mM NaCl which slightly differs from the wild-type buffer which used 20 mM Tris-Cl instead of KP_i . This alteration in the buffer was made to create a more stable environment for the enzyme during storage.

Circular Dichroic Analysis of PA1024-P78G

Circular dichroism was used as a means to compare the secondary structures of wild-type PA1024 and NQO-P78G to establish if NQO-P78G was folded properly with respect to the wild-type. Figure 3 shows that the far-UV circular dichroic spectra of the NQO-P78G and wild-type PA1024 determined at pH 7.0 and 25 °C are very similar to one another, both containing a single negative peak around 222 nm with a shoulder around 210 nm. Between the two enzymes there is a difference of $-0.22 \times 10^6 \text{ deg cm}^2 \text{ dmol}^{-1}$ at 222 nm and $-0.16 \times 10^6 \text{ deg cm}^2 \text{ dmol}^{-1}$ at 210 nm. Wild-type PA1024 absorbs slightly more right-handed circularly polarized light than the mutant however visually, this difference is not significant. PA1024's secondary structures composition contains more α -helices than β -strands and consequently the spectra presented are consistent with the distinct spectra exhibited by α -helices³³. Results are indicative that the two enzymes give the comparable CD responses at the far-UV region.

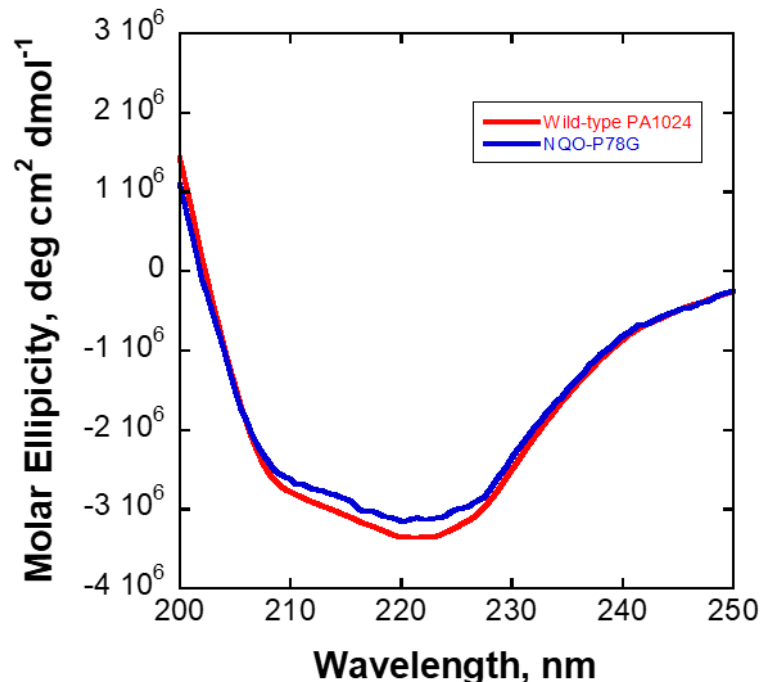


Figure 3. Circular dichroic spectra of wild-type PA1024 (red) and NQO-PA1024 (blue) were determined in 20 mM potassium phosphate (pH 7.0) and 200 mM sodium chloride at 25 °C. Far-UV spectra was measured from 200 – 250 nm due to the large salt concentration needed to prevent the enzyme from denaturing. Spectra were obtained from a single scan at a scan speed of 20 nm/min, data pitch of 0.5 nm, and D.I.T of 0.5 s. Data was analyzed and smoothed, by the Means-Movement method, using Jasco Spectra Analysis software.

Apparent Steady-State Kinetics

As a first step in the investigation on the effects of a P78G mutation the $^{app}k_{cat}$ value was determined by measuring initial rates of reaction at varying concentrations of benzoquinone and a saturating concentration of NADH at 100 μ M. Substrates were chosen based on previous wild-type PA1024 kinetic studies that determined the enzyme has the greatest catalytic efficiency with benzoquinone and NADH as the oxidizing and reducing substrates respectively²⁵. The concentrations of substrates used for NQO-P78G experiments were chosen based on previous wild-type PA1024 experiments which measured an $^{app}K_{benzoquinone}$ value of $15 \pm 1 \mu$ M and determined NADH is fully saturating the enzyme at 100 μ M²⁵. In contrast to wild-type PA1024, certain steady-state kinetic parameters for NQO-P78G could not be measured since the estimated

$^{app}K_{\text{benzoquinone}}$ value was too low for accurate kinetic determination of $^{app}K_{\text{benzoquinone}}$ and $^{app}(k_{\text{cat}}/K_{\text{benzoquinone}})$. NQO-P78G also differs from wild-type PA1024 at concentrations of benzoquinone greater than 21 μM where a decrease in initial rates is measured suggesting NQO-P78G is subject to substrate inhibition at high concentrations of benzoquinone. An $^{app}k_{\text{cat}}$ value of $1.4 \pm 0.2 \text{ s}^{-1}$ was obtained for NQO-P78G by averaging all initial rate values measured at saturating benzoquinone (Table 2). A comparison of identical apparent steady-states done on wild-type PA1024 and NQO-P78G measured an overall significant decrease in initial rates due to the P78G point mutation (Figure 4).

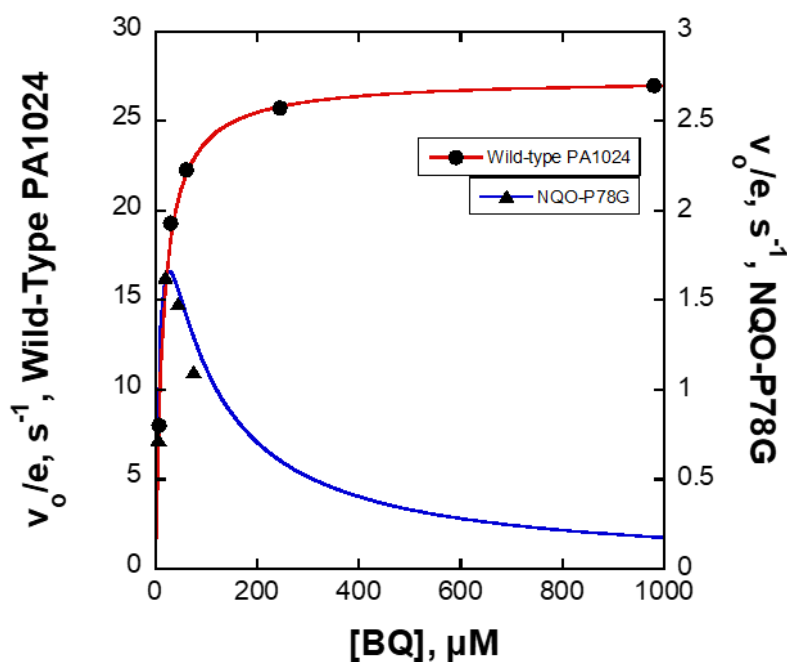


Figure 4. Initial rates of NADH consumption were measured at a fixed concentration of NADH (100 μM) and varying concentrations of benzoquinone from 3-100 μM . The experiment was done in 20 mM KPi , 200 mM NaCl , pH 7.0, at 25 $^\circ\text{C}$, and in triplicate with the average values being shown. Wild-type PA1024 was fit with the Michaelis-Menten equation for one substrate (Equation 1) while NQO-PA1024 was fit with the Michaelis-Menten equation for substrate inhibition (Equation 2).

Table 2. Summary of Apparent Steady-state Kinetic Parameters for Mutant and Wild-type PA1024

Enzyme	$^{app}k_{cat}$ (s^{-1})	$^{app}K_{benzoquinone}$ (μM)	$^{app}(k_{cat}/K_{benzoquinone})$ ($M^{-1} s^{-1}$)
Wild-Type PA1024	27 ± 1	15 ± 1	$1,900,000 \pm 130,000$
NQO-P78G	1.4 ± 0.2	$\leq 1^\ddagger$	$\geq 1,400,000^\ddagger$

[†]Values were estimated by analyzing the change in absorbance at the NADH absorbance peak.

Wild-type PA1024 and NQO-P78G were tested in 20 mM KP_i , 200 mM NaCl, pH 7.0, at 25 °C. Steady-state parameters were found by following the reduction of NADH at a saturating concentration of 100 μM and using the extinction coefficient for NADH at 340 nm ($\epsilon_{340} = 6,220 M^{-1} cm^{-1}$).

Steady-State Kinetics with NAD(P)H

The steady-state kinetic parameters for the mutant enzyme with NADH and NADPH were measured and compared at substrate concentrations ranging from 30 to 300 μM at pH 7.0 and 25 °C. In contrast with the previous apparent-steady state; this experiment measured true kinetic parameters using a derivation of the Michaelis-Menten equation for two substrates (Equation 3). A K_{NADH} value of 1200 μM was measured however concentrations of NADH greater than 300 μM could not be reliably tested using the spectrophotometer as the entire NADH peak was above 1 absorbance unit. This meant that K_{NADH} and k_{cat} could not be reliably measured however a k_{cat}/K_{NADH} value of $11,000 \pm 700 M^{-1} s^{-1}$ was determined (Figure 5A). It was possible to measure concentration dependence on initial rate for NAO-P78G only when NADH was the reducing substrate (Figure 5). NADPH as the reducing substrate saw no enzymatic reaction with NQO-P78G.

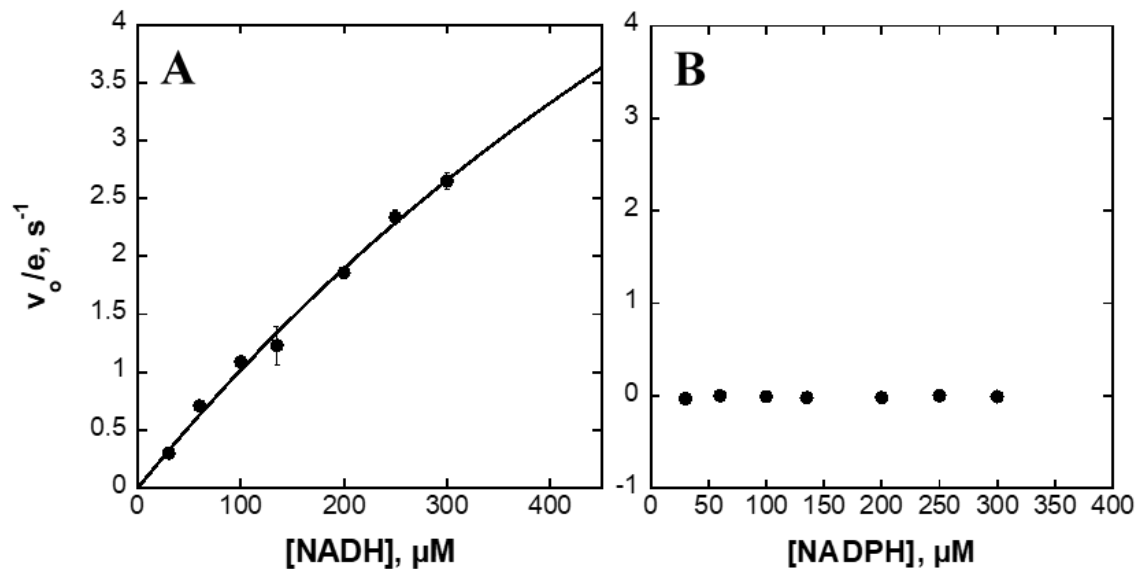


Figure 5. Concentration dependence of the initial rate of reaction of NQO-P78G while varying NADH (A) and NADPH (B) from 30 – 300 μM . Steady-state experiments were done in a fixed concentration of benzoquinone at 21 μM and in 20 mM KPi, 200 mM NaCl, pH 7.0 and 25 °C. Data points were tested in triplicate with the average values and corresponding standard deviations being shown. The curve for NADH was obtained by fitting the data with the Michaelis-Menten equation (Equation 3).

Discussion

Crystal structures of wild-type PA1024 suggest that steric hindrances stemming from mobile loop residues P78 and Q80 could be the cause of the reducing substrate specificity found for the enzyme³⁰. Previous rapid kinetic studies on wild-type PA1024 determined NADH is the preferred reducing substrate by measuring a k_{cat} value that was at least ~3,500 times faster with NADH, compared to NADPH²⁵. The structural determinants for NADH specificity were tested through crystallographic studies which observed a mobile loop that undergoes a conformational change of 5.5 Å towards the active site³⁰. This conformation change is thought to occur sometime during NADH binding. The mobile loop's closed conformation was modeled in complex with NADP⁺ while different conformations of the phosphate group in NADPH were tested³⁰. This theoretical model suggested P78, located on the mobile loop, was partially inhibiting NADPH from forming a complex with wild-type PA1024 by sterically hindering the 2' phosphate of NADP⁺'s adenine

moiety. P78 was found to be highly conserved among ~500 hypothetical proteins that share the same conserved motifs as wild-type PA1024 further suggesting the proline plays a necessary role in NADH:quinone oxidoreductases²⁵. In this study mutagenesis, protein purification and expression, circular dichroism, and steady-state kinetic approaches were utilized to test the role of P78 in creating a reducing substrate specificity in PA1024.

From a wild-type pET20b(+)/*pa1024* plasmid in *E. coli*, a *pa1024*-P78G variant was prepared via site-directed mutagenesis and the recombinant protein NQO-P78G was purified to a high yield for subsequent experiments. Evidence of a successful mutation comes from a sequence analysis of the mutated plasmid while NQO-P78G purification and expression was confirmed through activity assays and SDS-PAGE analysis. Among all the amino acids, proline is the only amino acid to contain a side chain that covalently binds to the peptide backbone. By binding to the peptide backbone proline can provide stability to the surrounding backbone and prevent certain secondary structures, such as α -helices, from forming^{34, 35}. P78 was mutated to a glycine to remove the steric hindrances from residue 78 as well as some rigidity from the mobile loop which potentially assists in stabilizing the mobile loop conformations. The resulting loss of rigidity on the mobile loop from mutagenesis was not a concern as other prolines are found on the mobile loop at residues 82 and 84. A P78G mutation was prepared because glycine has the shortest side chain among the amino acids, sporting just a hydrogen as a side chain. Replacement of proline's cyclic side chain with a hydrogen reduces the steric hindrances found at residue 78 thus allowing the role of P78 in preventing NADPH from binding to the active site of PA1024 to be tested. Wild-type PA1024 and NQO-P78G were tested for variations in substrate specificity to measure the impact of a loss in steric hindrances and rigidity at residue 78. NQO-P78G was expressed and purified in the same manner as wild-type PA1024.

A P78G mutation did not result in any significant changes to the overall structure of the enzyme with respect to wild-type PA1024. Evidence of this conclusion comes from circular dichroism studies comparing wild-type PA1024 and NQO-P78G in the far-UV region (200-250 nm). Circular dichroic spectra of wild-type PA1024 and NQO-P78G are comparable to one another which confirms a P78G mutation did not affect the secondary structure content of PA1024 (Figure 3). The complete far-UV spectra (180-250 nm) could not be measured because both forms of PA1024 requires a high salt concentration to remain in solution which interfered with the CD response around the 180–200 nm region. However, the full far-UV spectra is not required since CD unfolding studies are commonly done at 222 nm which is unaffected by a high salt buffer³³. Absorbance of circularly polarized light at the 222 nm peak is also used to assess the α -helical content of proteins³³. PA1024 contains 14 α -helices throughout its structure thus the 222 nm peak is a good indicator for comparing the overall secondary structure folding of wild-type PA1024 and NQO-P78G³⁰. The P78G mutation resulting in no structural changes is consistent with previous TIM-barrel domain studies that suggest mutations on $\beta\alpha$ loops do not jeopardize the stability of the enzyme⁶. Overall, the P78G mutation had no significant effects on the structure of the enzyme in comparison to the wild-type.

A P78G mutation on PA1024 significantly decreases the ability of the enzyme to turnover with preferred substrates. Evidence to support this conclusion comes from an apparent steady-state on NQO-P78G that measured initial rates at various concentrations benzoquinone and a saturating concentration of NADH. A 20-fold decrease in the $^{app}k_{cat}$ value was measured and a 15-fold decrease in the $^{app}K_{benzoquinone}$ value was estimated for NQO-P78G compared to that of wild-type PA1024. In the case of wild-type PA1024, benzoquinone was found to be the preferred oxidizing substrate after relatively large $^{app}k_{cat}$, $^{app}K_{benzoquinone}$, and $^{app}(k_{cat}/K_{benzoquinone})$ values were measured

and compared to various quinones²⁵. Comparison of wild-type PA1024 kinetic parameters to the kinetic parameters measured for NQO-P78G in this study demonstrate P78 plays a key role in maintaining an efficient turnover rate and possibly substrate affinity (Table 2). An observed decrease in the $^{app}(k_{cat}/K_{benzoquinone})$ value was estimated as well. However, unlike the other kinetic parameters, this was a 1.1-fold decrease when compared to wild-type PA1024, which implies that the catalytic efficiency of PA1024 is not affected by a P78G mutation. Previous studies established that steady-state kinetic parameters at varying concentrations of benzoquinone and a fixed concentration of NADH were determined by using the Michaelis-Menten equation for one substrate (Equation 1)²⁵. However, NQO-P78G is subject to substrate inhibition at relatively low concentrations of benzoquinone thus steady-state kinetic parameters for NQO-P78G were measured using a variant of the Michaelis-Menten equation which considers substrate inhibition (Figure 4, Equation 2). Results elucidate the importance of P78 by suggesting the role of this proline is to assist in maintaining efficient enzymatic rates.

Reducing the steric hindrance at residue 78 did not alter the reducing substrate specificity of PA1024 so that NADPH could act as a substrate. Evidence to support this conclusion comes from steady-state kinetic experiments with NQO-P78G that measured a concentration dependence of enzymatic rates with NADH and an absence of enzymatic turnover with NADPH (Figure 5). These results are consistent with previous wild-type PA1024 steady-state experiments which also measure insignificant turnover rates with NADPH when compared to NADH. In contrast, NQO-P78G is not capable of reaching saturating concentrations of NADH during in vitro studies whereas wild-type PA1024 is saturated at 100 μ M NADH. The estimated $^{app}K_{benzoquinone}$ for NQO-P78G was found to be sufficiently low enough to allow the Michaelis-Menten equation to be manipulated resulting in the measurement of true kinetic parameters (Equation 3). However, this

is not the case for wild-type PA1024 thus the measured $k_{\text{cat}}/K_{\text{NADH}}$ value of $11,000 \pm 700 \text{ M}^{-1} \text{ s}^{-1}$ has no direct comparison to wild-type PA1024 at the moment. Ultimately, this experiment proves the hypothesis to be incorrect by measuring no change in reducing substrate specificity following a P78G mutation.

Conclusion

In summary, we have used site-directed mutagenesis, protein purification and expression, circular dichroism, and steady-state kinetics to suggest that the role of the highly conserved P78 in PA1024 is to maintain efficient enzymatic rates during turnover. The most significant effect of a P78G mutation on PA1024 was a measured 20-fold and estimated 15-fold reduction in the kinetic parameters $^{\text{app}}k_{\text{cat}}$ and $^{\text{app}}K_{\text{benzoquinone}}$ respectively. This large decrease in kinetic parameters suggest the conserved role of P78 is involved in catalysis rather than the original assumption of substrate specificity. We propose the presence of P78 in NADH:quinone oxidoreductases maintains enzymatic rates by providing a rigidity to the mobile loop so that the microenvironment of the flavin cofactor remains favorable for turnover. Future studies are aimed at analyzing the microenvironment surrounding the FMN cofactor in NQO-P78G through CD studies as well as crystalizing the enzyme in ligand-free and ligand-bound forms for comparison with wild-type PA1024. The results presented on NQO-P78G show no change in substrate specificity which is in agreement with previous substrate specificity studies with wild-type PA1024. Thus, we can conclude that P78 does not fully control the reducing substrate specificity in PA1024. Since P78 has no effect on substrate specificity it is likely the steric hindrances stemming from Q80 prevent NADPH from reacting with wild-type PA1024 and NQO-P78G as efficiently as NADH. Additionally, it is possible the prolines at residues 82 and 84 continue to provide enough rigidity to the mobile loop to allow sterically hindering residues to position themselves properly to hinder

NADPH. By testing the role of the key residue (P78) from the recently defined class of NADH:quinone oxidoreductases; it is possible to better understand what important features nature has incorporated into protein structures to result in efficient enzymes.

References

- [1] Wierenga, R. K. (2001) The TIM-barrel fold: a versatile framework for efficient enzymes, *FEBS Lett.* 492, 193-198.
- [2] Copley, R. R., and Bork, P. (2000) Homology among (betaalpha)(8) barrels: implications for the evolution of metabolic pathways, *J. Mol. Biol.* 303, 627-641.
- [3] Gerlt, J. A. (2000) New wine from old barrels, *Nat. Struct. Biol.* 7, 171-173.
- [4] Nagano, N., Hutchinson, E. G., and Thornton, J. M. (1999) Barrel structures in proteins: automatic identification and classification including a sequence analysis of TIM barrels, *Protein Sci.* 8, 2072-2084.
- [5] Hegyi, H., and Gerstein, M. (1999) The relationship between protein structure and function: a comprehensive survey with application to the yeast genome, *J. Mol. Biol.* 288, 147-164.
- [6] Hocker, B., Jurgens, C., Wilmanns, M., and Sterner, R. (2001) Stability, catalytic versatility and evolution of the (beta alpha)(8)-barrel fold, *Curr. Opin. Biotechnol.* 12, 376-381.
- [7] Petsko, G. A. (2000) Enzyme evolution. Design by necessity, *Nature* 403, 606-607.
- [8] Thanki, N., Zeelen, J. P., Mathieu, M., Jaenicke, R., Abagyan, R. A., Wierenga, R. K., and Schliebs, W. (1997) Protein engineering with monomeric triosephosphate isomerase (monoTIM): the modelling and structure verification of a seven-residue loop, *Protein Eng.* 10, 159-167.
- [9] Inouye, M. (2016) The first application of site-directed mutagenesis using oligonucleotides for studying the function of a protein, *Gene* 593, 342-343.
- [10] Jürgens, C., Strom, A., Wegener, D., Hettwer, S., Wilmanns, M., and Sterner, R. (2000) Directed evolution of a (beta alpha)8-barrel enzyme to catalyze related reactions in two different metabolic pathways, *Proc. Natl. Acad. Sci. U.S.A* 97, 9925-9930.
- [11] Michaelis, L., Menten, M. L., Johnson, K. A., and Goody, R. S. (2011) The original Michaelis constant: translation of the 1913 Michaelis-Menten paper, *Biochemistry* 50, 8264-8269.
- [12] Yan, S., and Wu, G. (2013) Predictions of enzymatic parameters: a mini-review with focus on enzymes for biofuel, *Appl. Biochem. Biotech.* 171, 590-615.
- [13] Ball, J., Bui, Q. V., Gannavaram, S., and Gadda, G. (2015) Importance of glutamate 87 and the substrate alpha-amine for the reaction catalyzed by D-arginine dehydrogenase, *Arch. Biochem. Biophys.* 568, 56-63.
- [14] Gadda, G., and Yuan, H. (2017) Substitutions of S101 decrease proton and hydride transfers in the oxidation of betaine aldehyde by choline oxidase, *Arch. Biochem. Biophys.* 634, 76-82.
- [15] Northrop, D. B. (1998) On the Meaning of Km and V/K in Enzyme Kinetics, *J. Chem. Educ.* 75, 1153.
- [16] Deller, S., Macheroux, P., and Sollner, S. (2008) Flavin-dependent quinone reductases, *Cell. Mol. Life Sci. : CMLS* 65, 141-160.
- [17] Iyanagi, T., and Yamazaki, I. (1970) One-electron-transfer reactions in biochemical systems. V. Difference in the mechanism of quinone reduction by the NADH dehydrogenase and the NAD(P)H dehydrogenase (DT-diaphorase), *Biochim. Biophys. Acta* 216, 282-294.
- [18] Brunmark, A., and Cadenas, E. (1989) Redox and addition chemistry of quinoid compounds and its biological implications, *Free Radic. Biol. Med.* 7, 435-477.
- [19] Ezraty, B., Gennaris, A., Barras, F., and Collet, J. F. (2017) Oxidative stress, protein damage and repair in bacteria, *Nature reviews. Microbiology* 15, 385-396.
- [20] Boland, M. P., Knox, R. J., and Roberts, J. J. (1991) The differences in kinetics of rat and human DT diaphorase result in a differential sensitivity of derived cell lines to CB 1954 (5-(aziridin-1-yl)-2,4-dinitrobenzamide), *Biochem. Pharmacol.* 41, 867-875.
- [21] Chen, S., Wu, K., and Knox, R. (2000) Structure-function studies of DT-diaphorase (NQO1) and NRH: quinone oxidoreductase (NQO2), *Free Radic. Biol. Med.* 29, 276-284.
- [22] Chen, H., Wang, R. F., and Cerniglia, C. E. (2004) Molecular cloning, overexpression, purification, and characterization of an aerobic FMN-dependent azoreductase from *Enterococcus faecalis*, *Protein Expr. Purif.* 34, 302-310.

- [23] Suzuki, Y., Yoda, T., Ruhul, A., and Sugiura, W. (2001) Molecular cloning and characterization of the gene coding for azoreductase from *Bacillus sp.* OY1-2 isolated from soil, *J. Biol. Chem.* 276, 9059-9065.
- [24] Ma, Q., Cui, K., Xiao, F., Lu, A. Y., and Yang, C. S. (1992) Identification of a glycine-rich sequence as an NAD(P)H-binding site and tyrosine 128 as a dicumarol-binding site in rat liver NAD(P)H:quinone oxidoreductase by site-directed mutagenesis, *J. Biol. Chem.* 267, 22298-22304.
- [25] Ball, J., Salvi, F., and Gadda, G. (2016) Functional Annotation of a Presumed Nitronate Monooxygenase Reveals a New Class of NADH:Quinone Reductases, *J. Biol. Chem.* 291, 21160-21170.
- [26] Ha, J. Y., Min, J. Y., Lee, S. K., Kim, H. S., Kim, D. J., Kim, K. H., Lee, H. H., Kim, H. K., Yoon, H. J., and Suh, S. W. (2006) Crystal structure of 2-nitropropane dioxygenase complexed with FMN and substrate. Identification of the catalytic base, *J. Biol. Chem.* 281, 18660-18667.
- [27] Salvi, F., Agniswamy, J., Yuan, H., Vercammen, K., Pelicaen, R., Cornelis, P., Spain, J. C., Weber, I. T., and Gadda, G. (2014) The combined structural and kinetic characterization of a bacterial nitronate monooxygenase from *Pseudomonas aeruginosa* PAO1 establishes NMO class I and II, *J. Biol. Chem.* 289, 23764-23775.
- [28] Le-Quoc, D., and Le-Quoc, K. (1989) Relationships between the NAD(P) redox state, fatty acid oxidation, and inner membrane permeability in rat liver mitochondria, *Arch. Biochem. Biophys.* 273, 466-478.
- [29] Mahler, H. R. (1954) Studies on the fatty acid oxidizing system of animal tissues. IV. The prosthetic group of butyryl coenzyme A dehydrogenase, *J. Biol. Chem.* 206, 13-26.
- [30] Ball, J., Reis, R. A. G., Agniswamy, J., Weber, I. T., and Gadda, G. (2019) Steric hindrance controls pyridine nucleotide specificity of a flavin-dependent NADH:quinone oxidoreductase, *Protein Sci.* 28, 167-175.
- [31] Matthews, R. G. (1986) Methylene tetrahydrofolate reductase from pig liver, *Methods Enzymol.* 122, 372-381.
- [32] Horecker, B. L., and Kornberg, A. (1948) The extinction coefficients of the reduced band of pyridine nucleotides, *J. Biol. Chem.* 175, 385-390.
- [33] Kelly, S. M., Jess, T. J., and Price, N. C. (2005) How to study proteins by circular dichroism, *Biochim. Biophys. Acta* 1751, 119-139.
- [34] Yu, H., and Huang, H. (2014) Engineering proteins for thermostability through rigidifying flexible sites, *Biotechnol. Adv.* 32, 308-315.
- [35] Yu, H., Zhao, Y., Guo, C., Gan, Y., and Huang, H. (2015) The role of proline substitutions within flexible regions on thermostability of luciferase, *Biochim. Biophys. Acta* 1854, 65-72.